

Damping and frequency changes induced by increasing levels of inelastic seismic demand

Diego A. Aguirre^{1a} and Luis A. Montejo^{*2}

¹Department of Civil Engineering and Surveying, University of Puerto Rico at Mayagüez,
Mayagüez PR 00681-9000, Puerto Rico

²Department of Engineering Science and Materials, University of Puerto Rico at Mayagüez
Mayagüez PR 00681-9000, Puerto Rico

(Received March 5, 2013, Revised April 20, 2014, Accepted April 29, 2014)

Abstract. The objective in this research is to determine the feasibility of using changes on the dynamic properties of a reinforced concrete (RC) structure to identify different levels of seismic induced damage. Damping ratio and natural frequency changes in a RC bridge column are analyzed using different signal processing techniques like Hilbert Transforms, Random Decrement and Wavelet Transforms. The data used in the analysis was recorded during a full-scale RC bridge column shake table test. The structure was subjected to ten earthquake excitations that induced different levels of inelastic demand on the column. In addition, low-intensity white noises were applied to the column in-between earthquakes. The results obtained show that the use of the damping ratio and natural frequency of vibration as damage indicators is arguable.

Keywords: damping ratio; natural frequency; reinforced concrete; bridge column; random decrement technique; wavelets; Hilbert Transform

1. Introduction

During a seismic event, a civil structure can be subjected to high inelastic demand and its dynamic properties can change depending on the resulting damage. If damage occurs, a decrease in its natural frequency and an increase in its damping ratio are expected. The main objective of this research is to assess the feasibility of employing the two aforementioned dynamic properties to identify different levels of seismic induced damage.

Various signal-based techniques for Structural Health Monitoring (SHM) purposes are based on the vibration characteristics of a structure. They are grounded on the premise that changes in the physical properties of a structure (i.e., mass, energy dissipation mechanisms, and stiffness) are directly related to changes in the modal properties, such as the natural frequencies, mode shapes, and modal damping (Curadelli *et al.* 2008). Therefore, the fundamental basis of these methods is that a local or global, stiffness, damping, or mass shift will induce changes in the modal parameters, and these changes can be used for damage identification. The aforementioned

*Corresponding author, Assistant Professor, E-mail: luis.montejo@upr.edu

^a Graduate Student, E-mail: diego.aguirre@upr.edu

parameters can be measured by performing time domain analyses, frequency domain analyses, or simultaneous time-frequency domain analyses.

The use of system identification for damage detection has been well studied in previous works in the field of SHM. Methodologies employing natural frequencies and damping ratios as damage indicators are summarized in Salawu (1997), Kareem and Gurley (1996), respectively. Banks *et al.* (1996), for instance, identified damage using frequency shifts using analytical and experimental results of small aluminum beam-like structures. Damping changes in aluminum beams were successfully detected by Kawiecki (2001) by employing the frequency transfer function, the proposed method is expected to work properly for light-weight and micro structures. Kullaa (2003) used changes in modal parameters to detect damage of the Z24 Bridge in Switzerland. He used stochastic subspace identification and ambient vibration test data in combination with statistical methods (control charts), which suggests a complex technique with the limitation that it was tested only to identify two damage stages. Zembaty *et al.* (2006) used experimental results obtained from two full-scale shaking table tests of reinforced concrete (RC) structures subjected to biaxial seismic excitations with increasing intensity levels. They performed dynamic identification analysis at different stages of damage; they found a decrease in the natural frequencies and an increase in the damping ratio. Todorovska and Trifunac (2007) analyzed data recorded from an instrumented six-story building severely damaged by the Imperial Valley EQ in 1979. They found changes (drops) in the instant frequencies of the building which were calculated by performing a time-frequency analysis of the seismic response of the structure, i.e. the changes they found were determined during the EQ excitation. Curadelli *et al.* (2008) performed laboratory tests and numerical simulations for two RC structures and one 3D steel frame. They found that damage causes important changes in damping, and then parameters that characterize structural damping can be used as damage-sensitive properties. For the modal identification they used, among others, the Wavelet Transform (WT) and Random Decrement Technique (RDT). Michel and Gueguen (2010) performed time-frequency analysis to detect frequency variations of two RC buildings subjected to strong and weak seismic excitations. They found frequency shifts during the strong earthquake's application; however, they also found that frequency variations under weak earthquakes are probably due to variations of the input motion. Loh *et al.* (2011) analyzed shaking table test data from six RC frames using a signal processing-based approach, among others, performing a system identification to support damage detection methodologies. While they were able to correlate the change in frequency with the inelastic demand in the structure, it should be noticed that the level of damage induced during the test remained on the serviceability level (e.g., no core crushing, no rebar buckling or rupture). One of the most recent studies was presented by Çelebi *et al.* (2012). They used records obtained from a 9-story building that was damaged during the March 11, 2011 Great East Japan Earthquake. They also used records obtained from the building two days before, during, and after the aforementioned mainshock to study changes in its dynamic properties. They found significant frequency shifts during the mainshock which correlate well with the observed damage in a column and some walls of the building. They also detect frequency shifts after repairs that were made two months after the mainshock.

In this work, changes in damping ratio and first natural frequency of a reinforced concrete (RC) structure were analyzed. There are some commonly used methods to identify such dynamic properties using free decay responses. The Fourier spectrum is frequently used to compute natural frequencies and it is highly accurate. In the case of damping ratios, the logarithmic decrement method is usually employed. Nevertheless, estimation of damping in structural systems has an intrinsic high variability due to the existence of many energy dissipation mechanisms (Kareem and

Gurley 1996). Other Fourier Transform-based approaches available to compute damping ratios (e.g., the half-power method) present difficulties in terms of frequency resolution, resulting in leakage problems increasing the uncertainty of results. In order to overcome the mentioned issues and the problems that arise with the presence of noise in experimental signals, time-frequency analysis based methodologies using free vibration responses have been presented by several authors (e.g., Ruzzene *et al.* 1997, Staszewski 1997, Lardies and Gouttebroze 2002, Kijewski-Correa 2003, Le and Argoul 2004, Curadelli *et al.* 2008, Chen *et al.* 2009, Ülker-Kaustell and Karoumi 2011, Le and Paultre 2012, Shi *et al.* 2012). In this article, system identification at different levels of induced damage will be performed using the Wavelet Transform (WT) and the Hilbert Transform (HT).

The data used in the analysis was collected during a full-scale RC bridge column shake table test recently performed at the Network for Earthquake Engineering Simulation (NEES) Large High Performance Outdoor Shake Table (LHPOST) at the University of California, San Diego (UCSD). Ten ground motions, starting with low-intensity motions, were applied to the column leaving it on near-collapse conditions. One of the safety columns was struck by the superstructure during the last Earthquake (EQ) load, and so this motion is not considered. In addition to earthquake loads, low-intensity White Noise (WN) excitations were applied to the column between earthquakes to identify dynamic properties. Natural frequencies and damping ratios were estimated before and after the ground motions are applied using the structural response to the low amplitude WNs and the portion of the response after each EQ load when the structure is in free vibration. For a better understanding and interpretation of the results, these parameters are then related with the maximum displacement ductility, the Damage Index (DI) and experimental observations during each earthquake.

The main contribution of this work can be summarized in three key points. First, while many of the studies found in the literature used small/reduced-scale structures, in this work experimental data from a real-scale reinforced concrete structure is used. Second, previous studies using actual structures or large scale tests commonly identify only few stages or levels of damage, the data used in this work provides the unique opportunity of analyzing the structure dynamic properties at several representative performance levels, from the pristine structure up to near collapse conditions. Finally, the results obtained set limitations not observed in early works for the use of frequency shifts for estimation of damage levels.

This document is organized as follows: the theoretical basis of the signal processing based system identification (i.e., the complex analytical signal, Random Decrement Technique (RDT), Hilbert Transform (HT), and Continuous Wavelet Transform (CWT)) is presented in section 2. Section 3 presents a description of the structure. Section 4 presents the fundamentals of the Damage Index (DI). Section 5 shows the results of applying the two approaches studied, and presents an analysis of the results considering the ductility and the calculated DI. Finally, the conclusions are presented in Section 6.

2. Signal processing based system identification

Two different approaches were employed to identify the structure natural frequency and damping ratio at the different test stages. In the first one, free decay response is obtained by applying the Random Decrement Technique (RDT) to the column acceleration response to white noise (WN) excitations to generate a Random Decrement Signature (RDS). The Hilbert Transform

(HT) is then applied to find the analytical signal. In the second approach, free decay response is obtained from the end portion of the column acceleration response to earthquake (EQ) excitations. In this case, the analytical signal is obtained by performing a Continuous Wavelet Transform (CWT) analysis. In order to be consistent, in both approaches the first natural frequency and damping ratio are computed from the analytical signal by applying linear fits as explained later.

2.1 The complex analytical signal

The analytical signal $z(t)$ (Gabor 1946) is a two dimensional signal composed of a real part and an imaginary part and it can be described by an exponential function given as

$$z(t) = x(t) + i y(t) = a(t)e^{i\theta(t)} \quad (1)$$

where

$$a(t) = \sqrt{x^2 + y^2} \text{ and } \theta(t) = \arctan\left(\frac{y}{x}\right) \quad (2)$$

where $a(t)$ and $\theta(t)$ are the instant amplitude (IA) and instant phase, respectively. The concept of instantaneous frequency as the time-varying derivative of the phase was proposed by Ville (1948) as

$$IF(t) = \frac{1}{2\pi} \frac{d}{dt} (\theta(t)) \quad (3)$$

Thus, the identification of the time-varying frequency of the system is provided by the phase of the complex analytic function. In this case, because the analyzed signal correspond to a free decay, the damped natural frequency (ω_d) is identified, and the amplitude term takes the form of an exponential which decays based on the natural frequency of the system (ω_n) and damping ratio (ξ). Eq. (1) then becomes

$$z(t) = (A_0 e^{-\xi \omega_n t}) e^{i(\omega_d t + \phi)} \quad (4)$$

where A_0 is an initial amplitude value, and ϕ is a phase shift. It should be noticed that if the IF is computed directly from Eq. (3), i.e., using numerical differentiation of instant phase values, the results obtained will show discontinuities at the same instants in which the instant phase presents discontinuities (Ramirez and Montejó 2011). This problem can be solved by using several techniques. One of them was proposed by Feldman (2011) and it consists of computing the phases of the differences instead of computing the differences of the phases

$$IF(t) = \frac{1}{2\pi} \text{Arg}[z_n \text{ conj}(z_{n+1})] \quad (5)$$

To obtain the complex analytical signal the HT or CWT can be employed as will be explained in sections 2.3 and 2.4. Having the analytical signal defined, the IA and IF are calculated using Eqs. (2) and (5), enabling the identification of the dynamic properties. During the signals analyzed in this study the natural frequency of the structure is not expected to change and therefore it can be estimated from the mean value of the IF or from the dominant peak in the amplitude Fourier spectrum. An average damping ratio is estimated by applying a linear fit to the natural logarithm of the instant amplitude as

$$\text{Ln}(IA) = -m \cdot t + \text{Ln}(A_0) \quad (6)$$

$$m = \xi \omega_n \quad (7)$$

where the resulting line slope (m) in Eq. (7) is computed from the linear fit. The structure average damping ratio and natural frequency can be calculated using Eqs. (8) and (9), respectively.

$$\xi = \frac{(m)^2}{\omega_d^2 + (m)^2} \quad (8)$$

$$\omega_n = \frac{\omega_d}{\sqrt{1-\xi^2}} \quad (9)$$

2.2 Random decrement technique

The Random Decrement Technique (RDT) is used to obtain the characteristic free decay of the structure from its response to WN, so that an average damping ratio can be estimated. RDT is a fast-converging method to extract information from random data. This method can be applied to any system which is subjected to an unknown random excitation in which only the system response is measured (e.g., the acceleration response). The fundamental concept of the RDT is based on the fact that the response of a damped structure is composed of two parts: a deterministic part and a random part (Al Sanad *et al.* 1983). Segments of the random vibration response of a system are ensemble averaged to form a signature that is representative of the free vibration modal response of the system. By averaging enough segments of the same random response, the random part will be averaged out, leaving the deterministic part (i.e., impulse and/or step function). The deterministic part that remains is the free vibration response from which the dynamic properties (i.e., the natural frequency and damping ratio) can be measured.

In order to explain the principles of the RDT, a linear single degree of freedom (SDOF) system will be analyzed. The displacement response $x_i(t)$ of a SDOF system that is subjected to an arbitrary load is governed by the following equation of motion

$$m \ddot{x}(t) + c \dot{x}(t) + k x(t) = f(t) \quad (10)$$

where $x(t)$, $\dot{x}(t)$, and $\ddot{x}(t)$ are the displacement, velocity, and acceleration responses, respectively. The parameters m , c , and k correspond to the mass, damping coefficient, and stiffness, respectively. Finally, $f(t)$ is an arbitrary excitation force which, in this particular case, must be of random nature. For linear systems the response $x_i(t)$ can be decomposed into three parts: response to initial displacement $x_d(t)$, response to initial velocity $x_v(t)$, and response to the random excitation force $x_f(t)$. The response can then be written as

$$x_i(t) = x_d(t) + x_v(t) + x_f(t) \quad (11)$$

The RDT consists of dividing a time history of a system response (i.e., displacement, velocity, or acceleration) into N equal length segments of duration τ_{max} possibly overlapping as illustrated in Fig. 1.

The starting time t_i of each segment is selected such that each one begins at a selected amplitude x_s . This means that $x_i(t_i) = x_s = \text{constant}$ and that the slope $\dot{x}_i(t_i)$ alternates between positive and negative. Segments are chosen such that half of them have initial positive slopes and half of them have initial negative slopes. These segments are then ensemble averaged to obtain a signature of length τ_{max} whose initial amplitude is x_s and which can be written as:

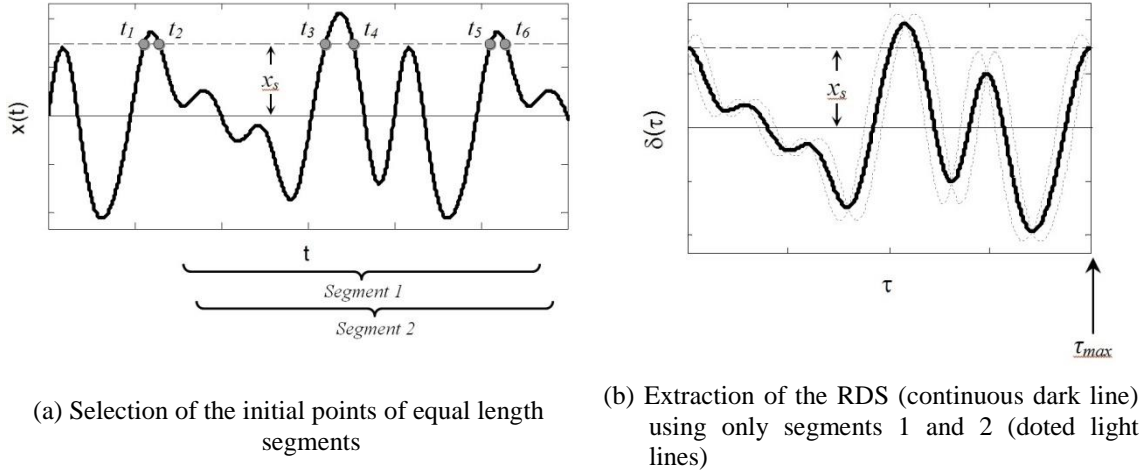


Fig. 1 Random decrement technique

$$\delta(\tau) = \frac{1}{N} \sum_{i=1}^N x_i(t_i + \tau) \tag{12}$$

where N is the number of segments, and $\delta(\tau)$ is a function called “the Random Decrement Signature” (RDS), which is defined in the time interval $0 \leq \tau \leq \tau_{max}$. Because the initial slopes alternate between positive and negative values, the average responses due to initial velocity cancel out. In addition, if the parts caused by the excitation force are averaged, they also disappear because the excitation is random with zero mean, Gaussian distribution by definition. The responses caused by initial displacement are left and their average is the random decrement signature which, for a linear SDOF system, represents the free vibration modal response of the system caused by an initial displacement, which corresponds to the initial value x_s . The required number of segments N to be averaged depends on the signal shape, but usually 400 to 500 segments are enough to obtain good results (Al Sanad *et al.* 1983).

One of the main advantages of this method is that it requires no knowledge of the excitation force $f(t)$, because of its random nature. As an example, Fig. 2 shows a low-intensity WN excitation and its corresponding simulated acceleration response of a damped SDOF system with natural frequency 2 Hz and damping ratio 2.5%. The RDT is applied to the acceleration response and the extracted RDS is illustrated in Fig. 3 as a continuous dark line.

An alternative way to obtain the Random Decrement Signature (RDS) is by estimating the Auto Random Decrement (ARD) functions, namely, the auto-correlation function from the random structural response (i.e., a stationary, zero mean, Gaussian distributed process). The Auto Random Decrement Signature (ARDS) $\delta_{xx}(\tau)$ of the structural response $x(t)$ is proportional to the auto-correlation function $R_{xx}(\tau)$ (Brincker *et al.* 1991, Lin and Chiang 2012), and it can be computed as

$$\delta_{xx}(\tau) = \frac{R_{xx}(\tau)}{R_{xx}(0)} \cdot x_s \tag{13}$$

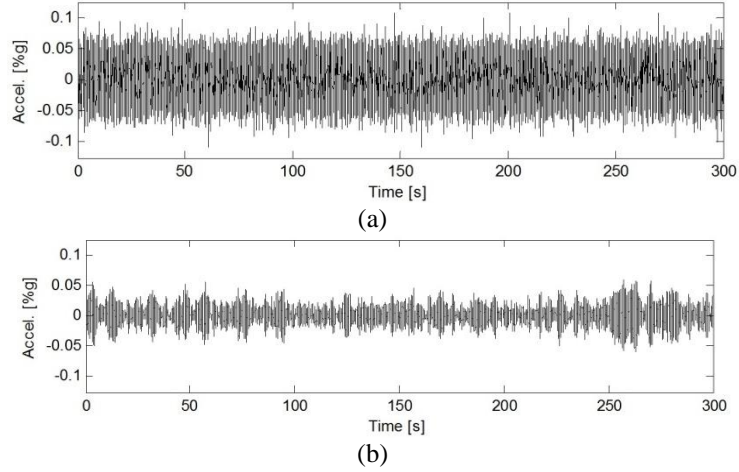


Fig. 2 (a) Generated low-intensity white noise excitation and (b) simulated acceleration response of a damped SDOF system

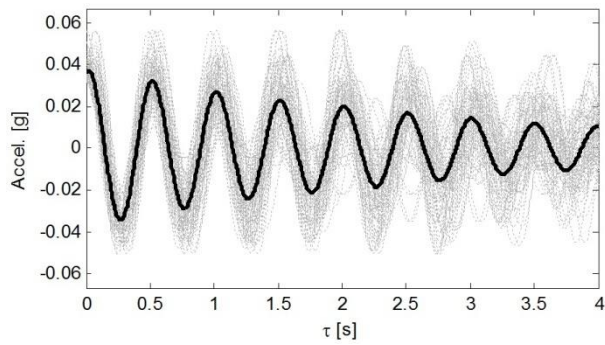


Fig. 3 Extracted RDS (continuous dark line) from the segments (dotted light lines) after applying the RDT to the simulated acceleration response of a damped SDOF system

where $R_{xx}(\tau)$ is the auto-correlation function of the signal $x(t)$ defined in the time interval $0 \leq \tau \leq \tau_{max}$, x_s is the initial amplitude, and $R_{xx}(0) = R_{xx}(\tau=0)$. Since the correlation function has the same mathematical form as that of the free vibration response (Lin and Chiang 2012) the ARDS can also be taken as the free vibration response for system identification purposes.

As an example, the RD function is computed for the simulated acceleration response $\ddot{x}(t)$ of the damped SDOF system illustrated in Fig. 2(b) and the result is presented in Fig. 4(a); for visualization purposes, only part of the response is shown. Fig. 4(b) shows the extracted ARDS using the same time interval used for the extracted RDS in Fig. 3. Notice that this free decay is proportional to the RD function but it is scaled according to the initial amplitude value x_s , which in this particular case is 95% of the signal's maximum amplitude. It is seen that the random decrement signature obtained using the two different approaches are quite similar (Figs. 3 and 4(b)); the amplitude differences are due to a tolerance criterion and the number of segments used to compute the RDS.

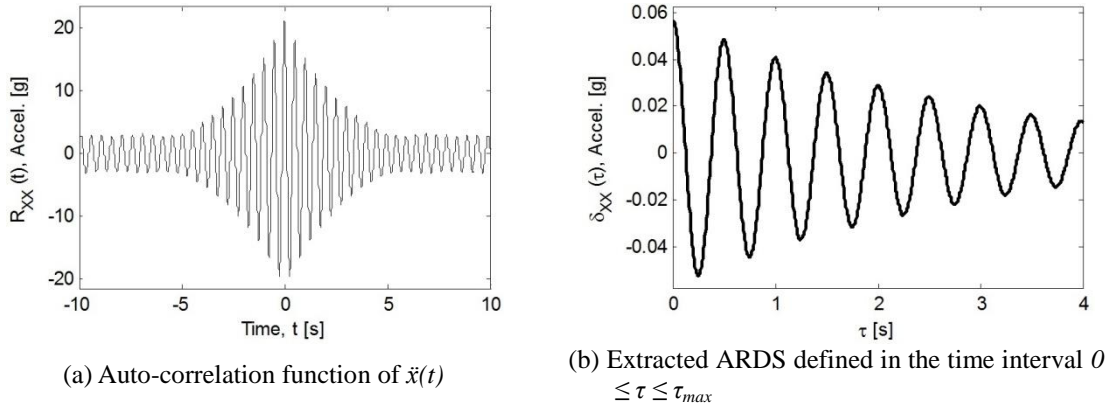


Fig. 4 Auto-correlation functions from the simulated acceleration response $\ddot{x}(t)$ (Fig. 2(b))

For multiple degree of freedom systems the response needs to be pre-processed to isolate all the modes in the response, which can be done by using methodologies like the Empirical Mode Decomposition (Huang *et al.* 1998), the Hilbert Vibration Decomposition (Feldman 2006), the Synchrosqueezed Transform (Daubuchies *et al.* 2011, Montejo and Vidot 2012) or band-pass filtering. The dynamic properties can then be estimated for each mode.

2.3 Hilbert transform

The Hilbert Transform (HT) of a function $x(t)$ is defined by an integral transform (Hahn 1996)

$$H[x(t)] = \frac{1}{\pi} \int_{-\infty}^{+\infty} \frac{x(\tau)}{t-\tau} d\tau \quad (14)$$

The HT is the convolution integral of the function $x(t)$ and the inverse of time, the result is the original signal with phase shift of $\pi/2$. The HT can then be used to generate the analytical signal (Eq. (1)) of the function $x(t)$

$$z(t) = x(t) + i y(t) = x(t) + i H[x(t)] = a(t)e^{i\theta(t)} \quad (15)$$

Given the HT it is possible to compute the IF and IA of a mono-component signal, allowing the identification of the natural frequency and damping ratio. Nevertheless, if the HT is applied to a multi-component signal it will still identify only one IF, which represents a weighted average of the frequencies occurring in the signal. Hence, for multi-component signals it is necessary to decompose them first into their mono-component constituents, using any of the methodologies mentioned in section 2.2.

Fig. 5 shows the calculation of the dynamic properties via HT from the free decay response of the damped SDOF system presented in Figs. 3 and 4(b). The natural frequency and the damping ratio identified were 2.01 Hz and 2.52%, respectively, by using the RDT (continuous dark line) and 232 segments with 4 seconds of duration; in this case, the error in the estimation of the parameters is less than 1%. By using the ARD function (dashed dark line), the natural frequency and damping ratio computed were 2.00 Hz and 2.82%, respectively; the error in the estimation of the damping ratio is 12.8%. Notice the edge effects at the beginning and end, an expected feature for any transform.

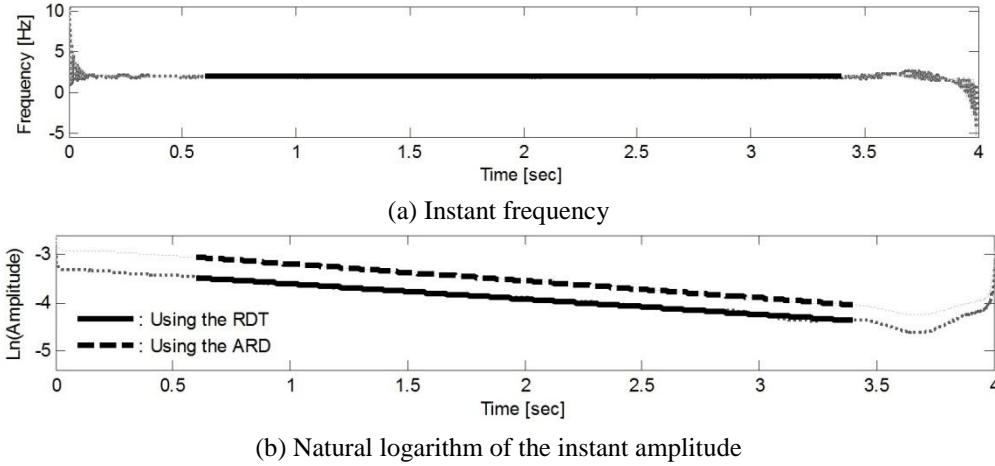


Fig. 5 Calculation of dynamic properties via HT

2.4 Continuous wavelet transform

The Continuous Wavelet Transform (CWT) allows performing a time-frequency analysis of a signal that can provide information about how the frequency content of the signal evolves with time (e.g., Montejó 2011, Montejó *et al.* 2012). The CWT of a function $x(t)$ of a real variable is defined as a function of two variables $W(a,b)$, which is the convolution of the signal and a scaled, shifted versions of the mother wavelet $\psi(t)$

$$W(a,b) = \frac{1}{\sqrt{a}} \int_{-\infty}^{+\infty} x(t) \psi\left(\frac{t-b}{a}\right) dt \quad (16)$$

The wavelet coefficients $W(a,b)$ are a measure of the similitude between the shifted mother wavelet and the signal at the time position b and scale a which can be related with frequency (Kijewski and Kareem 2003). A modified version of the Complex Morlet Wavelet (Grossman and Morlet 1990, Yan and Miyamoto 2006) is used in this research

$$\psi(t) = \frac{1}{\sqrt{\pi f_b}} e^{i 2 \pi f_c t} e^{-t^2/f_b} \quad (17)$$

where f_b is a bandwidth parameter that controls the shape of the mother wavelet and f_c is the central frequency of the mother wavelet. In this case, the time and frequency resolutions for this wavelet at a frequency f_i , using the Heisenberg uncertainty principle, are given by

$$\Delta t_i = \frac{f_c \sqrt{f_b}}{f_i^2} \text{ and } \Delta f_i = \frac{f_i}{f_c} \frac{1}{2 \pi \sqrt{f_b}} \quad (18)$$

Just as for the HT, it is necessary to find the analytical signal of the response function $x(t)$ in order to compute the dynamic properties of the system. In this case, because a complex wavelet is used, the wavelet coefficients obtained after a CWT analysis are also complex and the analytic signal can be extracted from them.

Usually, the wavelet coefficients $W(a,b)$ are illustrated in a two-dimensional graph as shown

in Fig. 6(b). This graph is called a wavelet map, and it is a representation of the response function $x(t)$ in the time-frequency domain. The darker colors indicate higher values of the wavelet coefficients. The estimation of the instant frequency is done by identifying a ridge in the time-frequency plane which can be obtained by locating the local maxima at each time instant (Montejó 2011). The ridge can be obtained according to

$$W(a_r, b) = \max[W(a, b)] \quad (19)$$

where a_r are the scales (that can be related to frequencies) corresponding to the ridge and $W(a_r, b)$ is a complex function that represents the ridge that evolves with time. The real and imaginary components along the ridge are directly proportional to the response function content at that frequency and its corresponding Hilbert transform (HT) (Kijewski and Kareem 2003). The analytical signal in Eq. (1) can be formed as

$$z(t) = W(a_r, b) = x(t) + i y(t) = a(t)e^{i\theta(t)} \quad (20)$$

Once the analytical signal is constructed, IF and IA can be computed to estimate the dynamic properties, as explained in section 2.1.

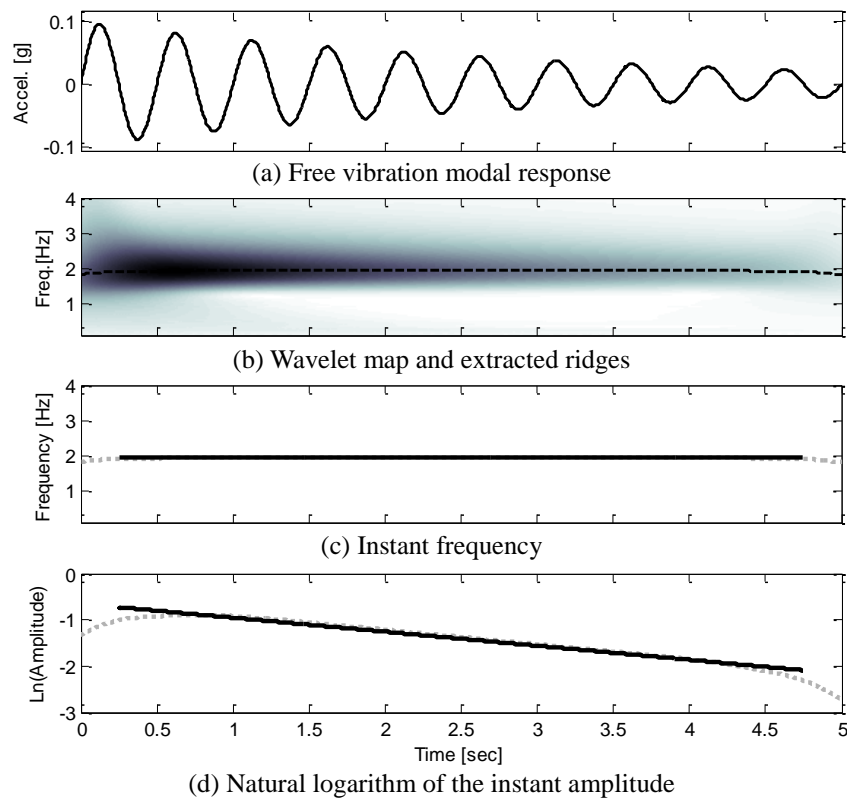


Fig. 6 Calculation of dynamic properties via CWT

Fig. 6 shows the calculation of the dynamic properties via CWT of the simulated free decay response of a damped SDOF system with a damping ratio of 2.50% and a natural frequency of 2 Hz. The calculated natural frequency and damping ratio identified were 1.94 Hz and 2.49%, respectively. In this case, the error in the estimation of the parameters is less than 3%. Edge effects appear at the beginning and the end as in the HT approach.

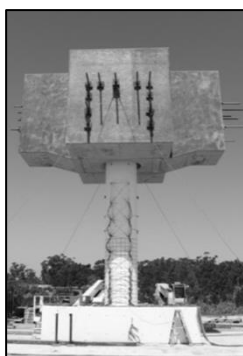
3. Test description

The RC bridge column was tested under uniaxial seismic excitation on the NEES-UCSD Large High Performance Outdoor Shake Table. The column had a height (cantilever length) of 7.32 m (24ft) with a circular cross section of 1.22 m (4ft) diameter, and it also had a reinforced concrete block at the top with a total weight of 2245 kN (250ton). A total of 18 No. 11 bars were provided as the longitudinal reinforcement and butt-welded double No. 5 hoops spaced 152 mm (6in) center to center were used as the transverse reinforcement. Further details of the test, material properties, and specimen geometry were presented by Schoettler *et al.* (2012). Fig. 7 shows schematic pictures of the test setup.

4. Damage index

A RC structure can be weakened or damaged when it is subjected to a combination of stress reversals and high stress excursions. Park and Ang (1985) proposed a damage model which includes not only the maximum response, but also the effect of repeated cyclic loadings. The seismic structural damage can be estimated as a Damage Index (DI) which is expressed as a linear combination of the damage caused by excessive deformation and that contributed by the repeated cyclic loading. Mathematically the DI can be calculated as follows

$$DI = \frac{\delta_M}{\delta_U} + \frac{\beta}{Q_Y \cdot \delta_U} \int dE \quad (21)$$



(a) Front view



(b) 3D view from bottom



(c) 3D view from top

Fig. 7 Full-scale RC bridge column test setup (photos taken from: <https://nees.org/warehouse/project/987/>)

where δ_M is the maximum deformation during an earthquake (i.e., a dynamic load), δ_U is the ultimate deformation, β is a non-negative parameter that represents the effect of cyclic loading on structural damage, dE is the incremental absorbed hysteretic energy, and Q_Y is the calculated yield strength but, if Q_U (i.e., the maximum strength) is smaller than Q_Y , then Q_Y is replaced by Q_U . The result of the integral in Eq. (21) is the total absorbed hysteretic energy (E) which can be determined by using the load-deformation time history. Fig. 8 illustrates the load, deformation, and load-deformation time history for the first ground motion (EQ1) applied during the full-scale test. The sum of the area of all hysteresis cycles from Fig. 8(c), allows calculating the total absorbed energy (E). Notice that the area of the hysteresis cycles is small which means that E will be also small, therefore, DI will be low for the EQ1. The dashed lines in Figs. 8(a) and 8(b) represent the yield strength and yield displacement, respectively. It can be observed, neither the lateral force nor the displacement exceed the yield limits aforementioned.

Structural damage is then a function of the responses δ_M and dE that are dependent of the load-deformation time history, while the parameters β , δ_U , and Q_Y are independent of it. The parameters δ_U , Q_Y , and Q_U can be obtained by performing a pushover analysis. Fig. 9 shows the simulated force-deformation curve for the column from which the ultimate deformation, yield strength, and maximum strength were $\delta_U = 106.1$ cm, $Q_Y = 611.7$ kN, and $Q_U = 482.8$ kN. Notice that $Q_U < Q_Y$, hence, according to the DI's definition, the yield strength must be replaced as $Q_Y = 482.8$ kN.

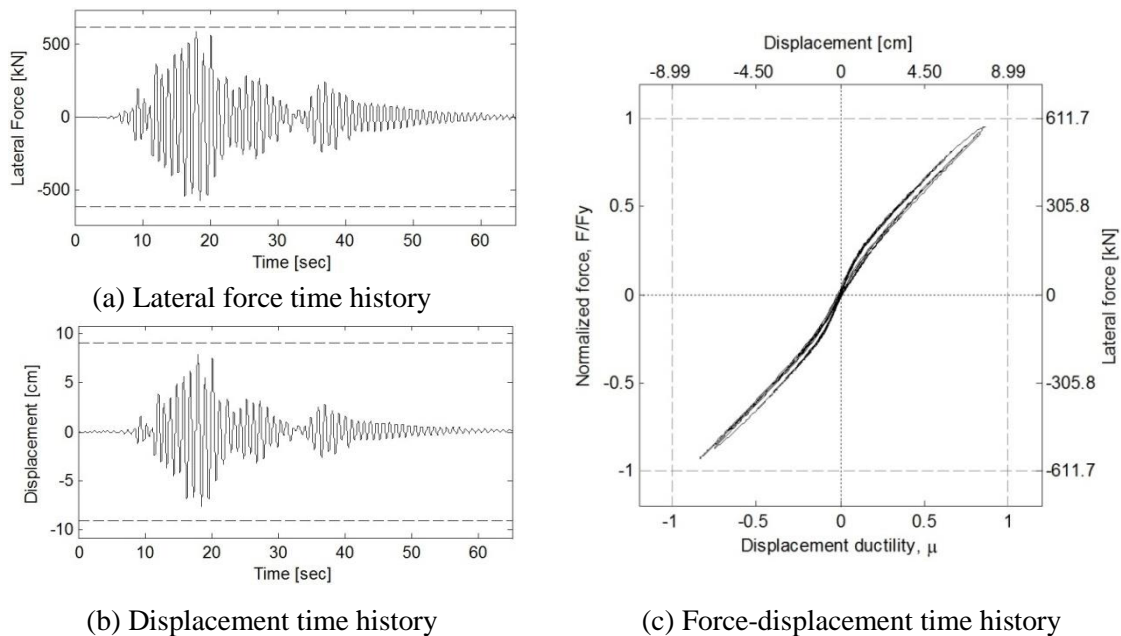


Fig. 8 Structure response during EQ1

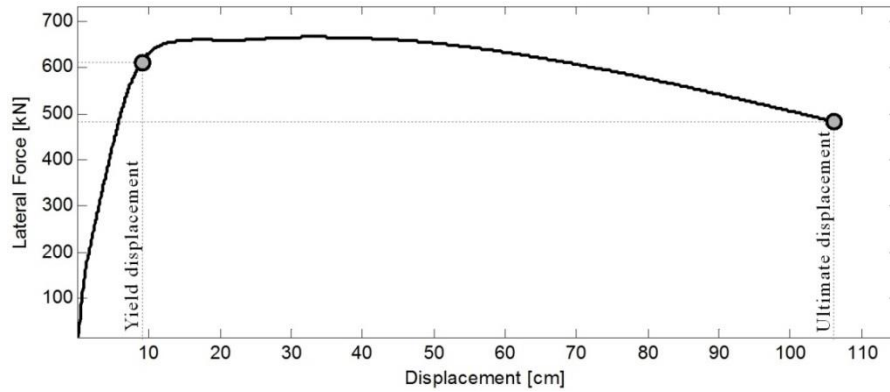


Fig. 9 Simulated monotonic force-deformation curve

The value of β can be obtained through a trial and error process by identifying different levels of performance. For example, if damage is induced such that the structure cannot be repaired then $DI \geq 1.0$. In this study, the load-deformation time history is known from the pristine structure up to near-collapse conditions, in other words, from $DI = 0.0$ to $DI \geq 1.0$. Moreover, the point of failure of the column was well-identified after the application of EQ7 due to the rebar buckling and the initial concrete core crushing.

Displacement and force time histories as well as results from a monotonic pushover analysis were obtained from a detailed distributed plasticity fiber based finite element model that closely resembled the behavior of the column. The structural model was generated using the OpenSees software framework system (McKenna *et al.* 2000). The model was subjected to monotonic pushover and dynamic analyses. In a fiber based approach the section of the column is represented by unidirectional fibers and constitutive-material relationships (i.e., material stress-strain behavior) are specified to each type of fiber. Further details of the nonlinear finite element model were presented by Aguirre *et al.* (2013).

In this work the DI is computed to analyze structural damage in a quantitative fashion, correlate it with the damage observed during the experimental tests, and for a better understanding and interpretation of the results obtained after performing system identification. In section 5.3, the DI is computed and then it is related with the frequency and damping changes of the structure.

5. Identification on a RC bridge column

In order to perform system identification analyses it is important to have a preliminary idea of the vibration characteristics of the analyzed signals. For this purpose, the normalized Fourier spectrum is computed using: (1) the column acceleration response to the WN excitations and (2) the free decay portion of the column acceleration response to the EQ excitations. Figs. 10(a) and 10(b) show the Fourier spectra for the column response before and after EQ1 and EQ9 are applied. A summary of the identified frequencies at each load stage is presented in Fig. 10(c). Notice that the shift in the natural frequency due to the induced damage is evident, from 1.2 Hz at the beginning of the tests to 0.43 Hz after the last EQ load application.

5.1 Identification using the response to white noises (RDT+HT)

As mentioned before, in this approach the identification is made using the response to low-intensity WN excitations. For the sake of brevity, only graphic results for WN1 and WN9 using the traditional RDT are displayed in Figs. 11-14. For all cases the segment duration varies in order to generate the RDS with the same number of cycles; a total of four cycles were used.

In the case of WN1, the natural frequency and damping ratio identified were 1.07 Hz and 3.26%, respectively, and a total of 206 segments with 3.66 seconds of duration were used to obtain the RDS. For the WN9, the natural frequency was 0.44 Hz, the damping ratio was 3.10%, and 186 segments with 9.09 seconds of duration were used. Notice that in some way the results in frequency changes are as expected, but the damping ratios seem to remain constant. Results for all the WNs analyzed and for the autocorrelation approach are presented in section 5.4

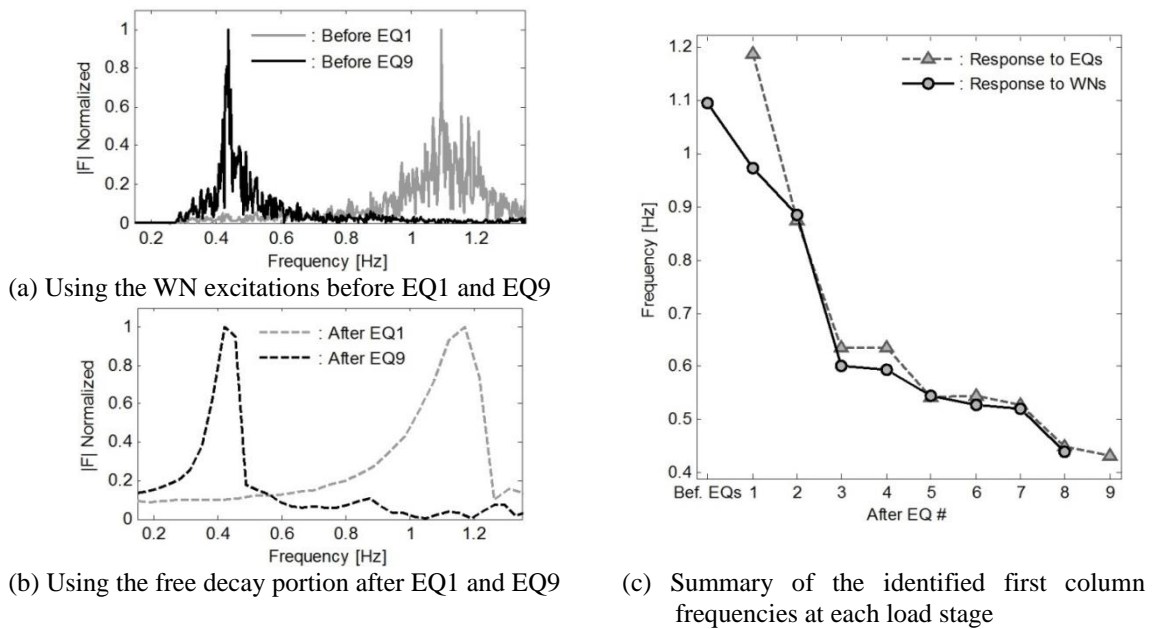


Fig. 10 Normalized Fourier spectra of the column acceleration response and summary of frequencies

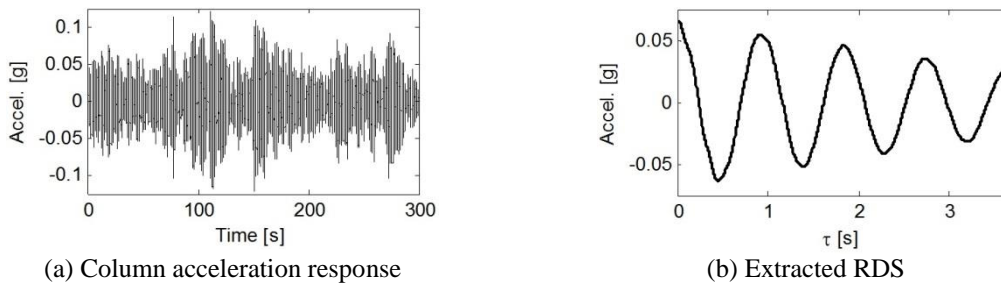


Fig. 11 Response and extracted RDS from the response to WN1

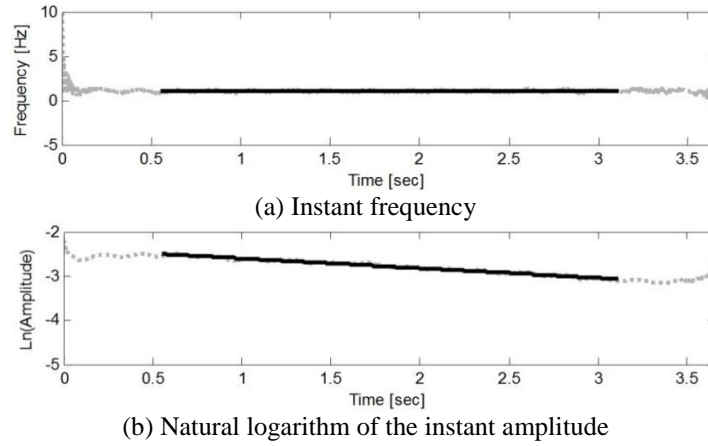


Fig. 12 Results of approach 1 for WN1 calculated from the free decay response in Fig. 11(b)

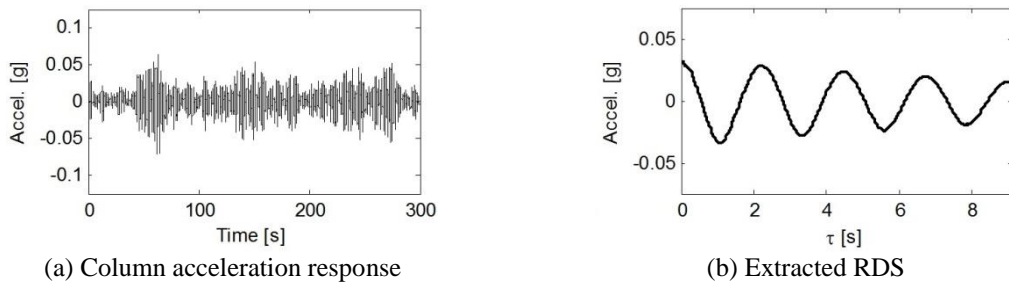


Fig. 13 Response and extracted RDS from the response to WN9

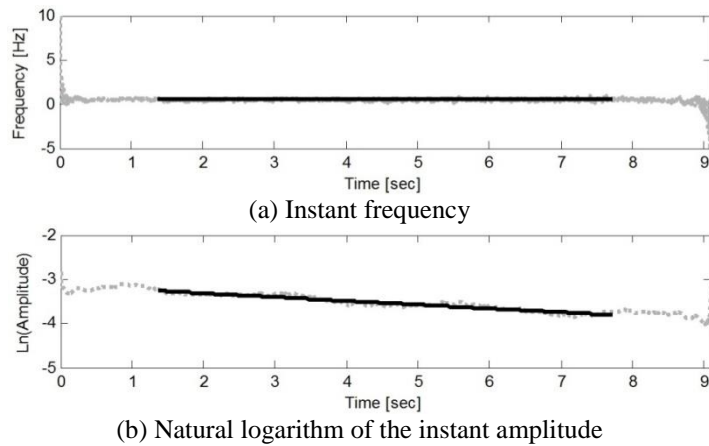


Fig. 14 Results of approach 1 for WN9 calculated from the free decay response in Fig. 13(b)

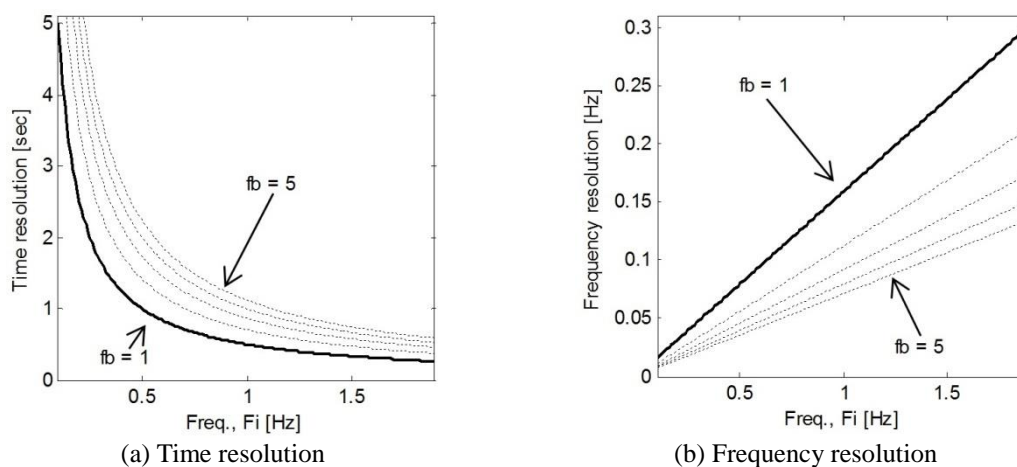


Fig. 15 Resolution for the modified Morlet Wavelet for different values of f_b and using $f_c=1$

5.2 Identification using free vibrations (CWT)

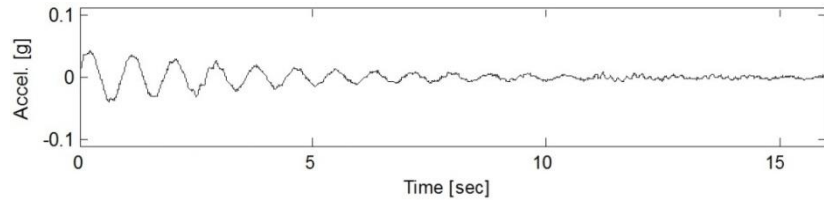
Before applying the CWT to the free decay portion of the column acceleration response to EQ load, it is necessary to define the frequency ranges for the analysis and define the wavelet parameters (i.e., the central frequency f_c , and bandwidth parameter f_b). From the Fourier analysis (Fig. 10(b)) it is known that the frequencies to identify vary from 1.19 Hz to 0.43 Hz after applying EQ9. Hence, the analyses were performed from 0.10 Hz to 1.90 Hz. Fig. 15 shows time and frequency resolutions as functions of frequency to be identified using the Heisenberg uncertainty principle. The selected parameters were $f_b=f_c=1$ for all cases.

Fig. 16 shows the results for the free decay portion after EQ1, and Fig. 17 presents the results for the free decay portion from EQ9. After EQ1 the natural frequency and damping ratio identified were 1.18 Hz and 2.83%, respectively. The natural frequency was 0.43 Hz and the damping ratio was 4.94% after EQ9 was applied. Results for all the EQs analyzed are presented in section 5.4.

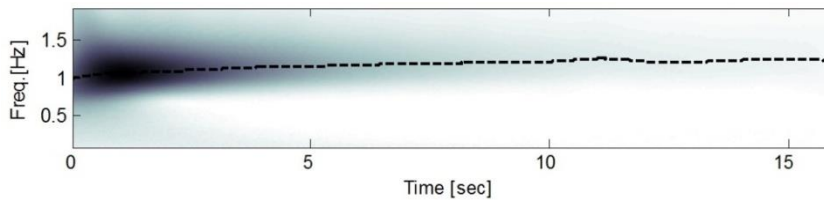
5.3 Damage index calculation

The ultimate deformation (δ_U), yield strength (Q_Y), and maximum strength (Q_U) are some of the parameters required to compute the DI; they were obtained previously in section 4. The maximum deformation (δ_M) and the parameter E, which is the integral in Eq. (21), need to be computed for each earthquake. Fig. 18 presents the maximum response and maximum displacement ductility for each ground motion.

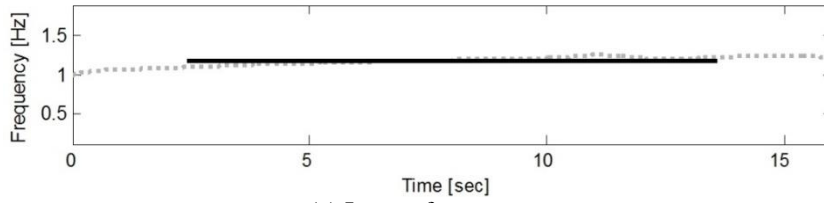
In the case of the total absorbed hysteretic energy (E), notice that it must be accumulated along all ground motions, for instance, for the EQ2 the total energy (E) is the sum of the hysteresis cycles of EQ2 and the energy previously calculated for EQ1, and so forth. Fig. 19 presents the absorbed hysteretic energy computed from all the hysteresis cycles of each EQ load. Given that for the experimental data only acceleration and displacement responses were available, the parameter E was computed using simulated force and displacement time histories as well as experimental accelerations and displacements.



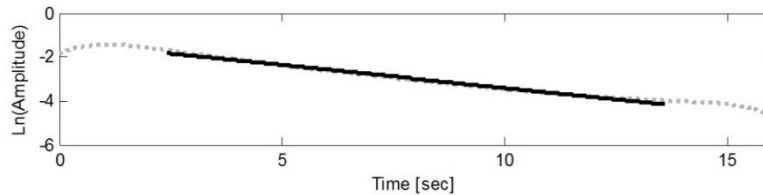
(a) Free decay portion



(b) Wavelet map and extracted ridges



(c) Instant frequency



(d) Natural logarithm of the instant amplitude

Fig. 16 Results of approach 2 for EQ1

Fig. 19(a) presents a normalized version of the absorbed energy (E) for comparison purposes. In both cases the normalization was performed based on the maximum value obtained in each case. Notice that, since the structure response is highly dominated by its first mode, the results obtained are strongly correlated. Fig. 19(b) shows the accumulated energy at each load stage; these values are used later to calculate DIs using Eq. (21). The value for the parameter beta ($\beta = 0.06$) was set so that the DIs obtained correlate well with the damage observed during the test. For example, after EQ7 when multiple rebar buckling and core crushing was observed, DI should be close to 1. On the other hand, for the first two records DI should be below 0.3 because the induced damage was negligible. The DI values computed after each EQ are presented in Fig. 20.

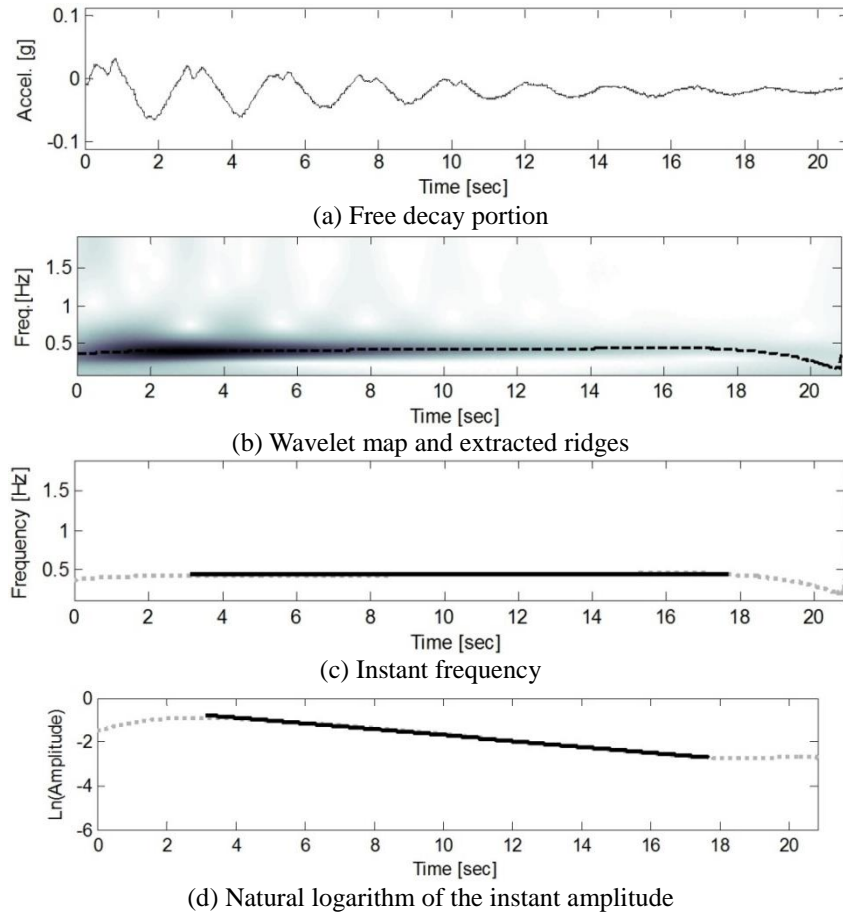


Fig. 17 Results of approach 2 for EQ9

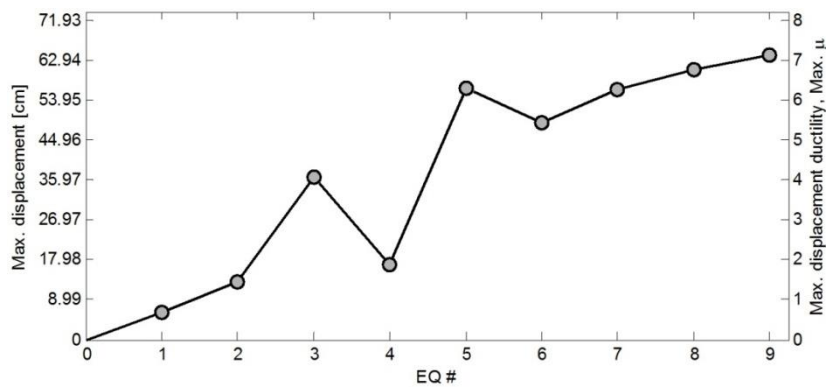
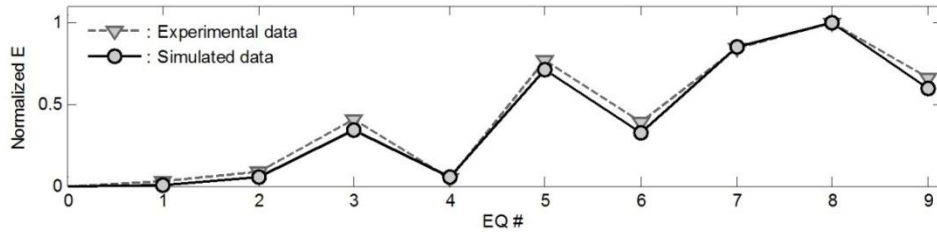
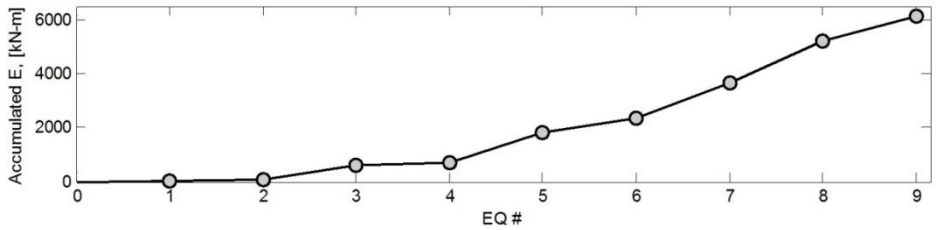


Fig. 18 Maximum response during each earthquake applied



(a) Normalized energy during each EQ load



(b) Accumulated normalized total energy at each load stage

Fig. 19 Absorbed hysteretic energy (E)

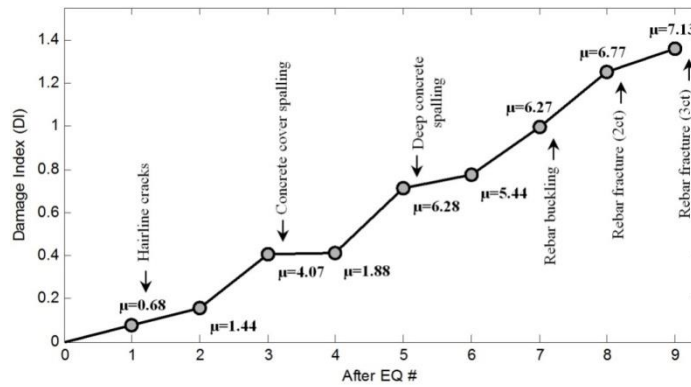


Fig. 20 Calculated damage index (DI) after each earthquake

5.4 Analysis of results

Fig. 21 summarizes the frequency shifts the structure experienced during the tests, it can be seen that the changes in the natural frequency are in close agreement for both approaches. There is some difference in the frequency values obtained for the structure after the first earthquake, but thereafter the frequencies identified are very similar. The largest frequency shift occurred for EQ3, just when the first substantial inelastic excursions occurred. From this point forth, the changes are less noticeable despite the increasing inelastic demand and induced damage during the following ground motions. The next observed frequency shifts (though much less significant) occurred for EQ5 which coincides with the observed deep concrete spalling and the on-set of buckling, and during EQ8, which coincides with the first rebar fractures. Table 1 summarizes and correlates the computed frequencies with the observed damage.

As can be seen from Fig. 22, differences in the results of the damping ratios identified by the three methodologies employed are larger than in the case of the natural frequencies. In this case results using the Auto Random Decrement (ARD) functions are also presented. A minimum of 200 segments and initial amplitude (x_s) equal to the maximum value of each WN acceleration response were used to compute the RDS in the RDT approach. It is seen that the estimated damping ratios are below 5%, typical of reinforced concrete structures. However there are variations in the values estimated by each methodology and a correlation with the induced level of damage is not evident. While a relation between induced inelastic action and the structure dissipative properties is evident from the hysteretic energy plot on Fig. 19, the use of an equivalent viscous damping ratio to assess the structure condition after a damaging event is arguable.

Fig. 23 presents once more the frequency changes, but this time as function of the maximum displacement ductility reached during each EQ. Since the ground motions were not applied with increasing intensity levels, the results for EQ4, EQ6, and EQ7 are not shown. It is seen from Fig. 23 that while there is a clear tendency on the natural frequency to decrease as the inelastic demand increase, this behavior is almost asymptotic. That is, the changes in frequency are more notorious at the early stages of ductility demand (<4) and then tend to saturate unless a major sudden damage occur for the first time (in this case rebar fracture around ductility 6-7).

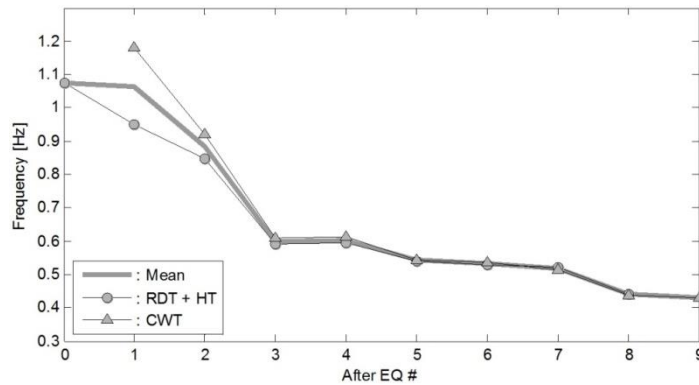


Fig. 21 Frequency changes after each earthquake for both approaches

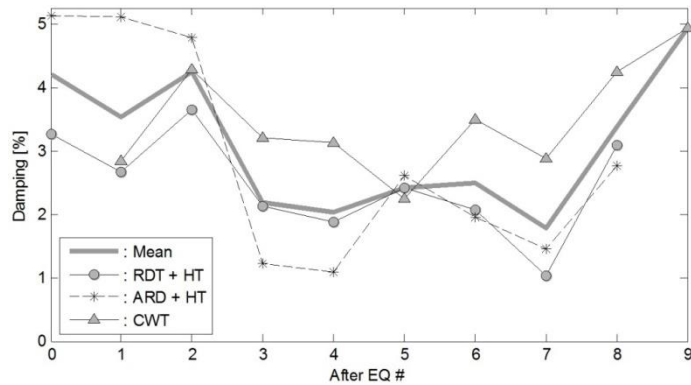


Fig. 22 Damping changes after each earthquake

Table 1 Significant performance levels and frequency shifts

Test	Damage	Relative Freq. Shift (%)	Absolute Freq. Shift (%)
EQ1	Hairline cracks	0.82	0.82
EQ2	No significant changes	17.08	17.76
EQ3	Concrete cover spalling	32.11	44.17
EQ4	No significant changes	0.62	43.82
EQ5	Deep concrete spalling	10.02	49.45
EQ6	No significant changes	2.09	50.51
EQ7	Rebar buckling	2.59	51.79
EQ8	Rebar fracture (2)	15.04	59.04
EQ9	Rebar fracture (3)	2.17	59.93

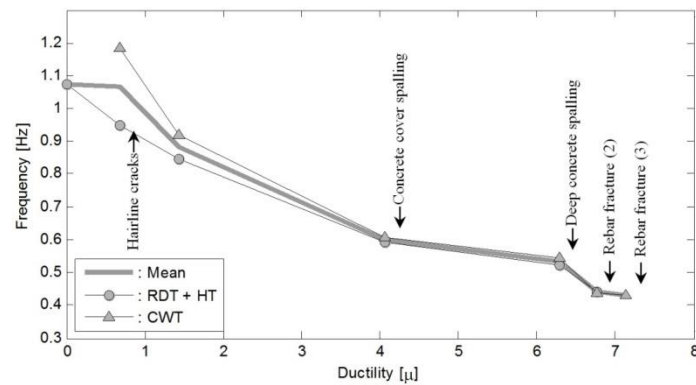


Fig. 23 Frequency changes vs. ductility demand for both approaches

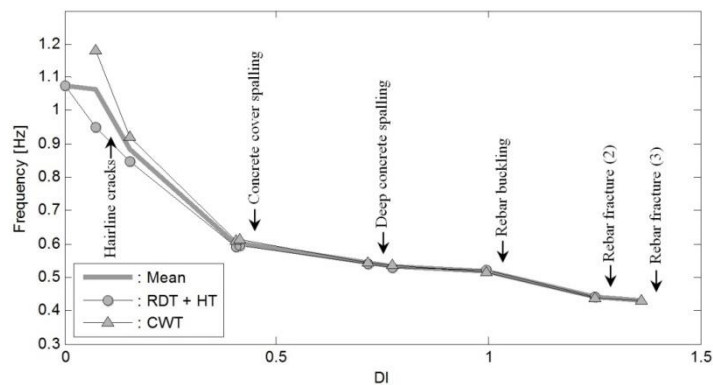


Fig. 24 Frequency changes vs. damage index (DI) for both approaches

6. Conclusions

The Random Decrement Technique (RDT) in combination with the Hilbert Transform (HT) and the Continuous Wavelet Transform (CWT) were the two approaches used in order to investigate the changes in dynamic properties in a RC bridge column. For the sake of brevity, the complete results for different number of segments and initial amplitude in the first approach (i.e., RDT + HT) are not presented. However, it was found that the results on computing RDS could be very sensitive to changes in these two parameters.

The results of the CWT analyses seem to be more stable than those of the RDT approach. Nevertheless, the selection of the free decay portion from the column response to EQ excitation plays an important role in the final results because one can disregard important data in the selection process. The results obtained show that a clear trend in damping ratio changes is not observed and thus this dynamic parameter does not seem to be a good damage indicator. Other methodologies should be explored in order to better identify the changes in the dissipative properties of the structure.

In regard to natural frequency, decreasing values were observed as the lateral demand in the column increased. However, the observed frequency shifts tend to saturate at large levels of ductility demand. Perhaps this parameter can be used as damage indicator for moderate damage (e.g., cracking and concrete spalling), however, its ability to differentiate moderate to severe damage (e.g., rebar buckling or rupture) is arguable.

Acknowledgements

This research is supported by the National Science Foundation Grant No. CMMI-1121146. The experimental data used in this work was obtained from the NEEShub Project Warehouse, a centralized data repository for sharing and publishing earthquake engineering research data from experimental and numerical studies (<https://nees.org/warehouse/project/987/>). The authors gratefully acknowledge to Dr. Matthew Schoettler and Professor Jose Restrepo at University of California, San Diego, for making the raw data for this set of tests publicly available in a timely manner.

References

- Aguirre, D.A., Gaviria, C.A. and Montejó, L.A. (2013), "Wavelet based damage detection in reinforced concrete structures subjected to seismic excitations", *J. Earthq. Eng.*, **17**(8), 1103-1125.
- Al Sanad, H., Aggour, M.S. and Yang, J.C.S. (1983), "Dynamic shear modulus and damping ratio from random loading tests", *Geotech. Test. J.*, **6**(3), 120-127.
- Banks, H.T., Inman, D.J., Leo, D.J. and Wang, Y. (1996), "An experimentally validated damage detection theory in smart structures", *J. Sound Vib.*, **191**(5), 859-880.
- Brincker, R., Krenk, S. and Jensen, J.L. (1991), "Estimation of correlation functions by the random decrement technique", *Proceedings of the Florence Modal Analysis Conference*, Florence, Italy.
- Çelebi, M., Okawa, I. and Kashima, T. (2012), "March 11, 2011 m=9.0 great east japan earth-quake: the story of a retrofitted building damaged and repaired", *Proceedings of the 15th WCEE*, Lisbon, Portugal, September.
- Chen, S.L., Liu, J.J. and Lai, H.C. (2009), "Wavelet analysis for identification of damping ratios and natural

- frequencies”, *J. Sound Vib.*, **323**(1-2), 130-147.
- Curadelli, R.O., Riera, J.D., Ambrosini, D. and Amani, M.G. (2008), “Damage detection by means of structural damping identification”, *Eng. Struct.*, **30**(12), 3497-3504.
- Daubuchies, I., Lu, J., Wu, H.T. (2011), “Synchrosqueezed wavelet transforms: an empirical mode decomposition-like tool”, *Appl. Comput. Harmon. A.*, **30**(2), 243-261.
- Feldman, M. (2006), “Time varying vibration decomposition and analysis based on the Hilbert transform”, *J. Sound Vib.*, **295**(3-5), 518-530.
- Feldman, M. (2011), “Hilbert transform in vibration analysis”, *Mech. Syst. Signal. Pr.*, **25**(3), 735-802.
- Feldman, M. (2011), *Hilbert Transform Applications in Mechanical Vibration*, John Wiley & Sons Ltd, The Atrium, Southern Gate, Chichester, West Sussex, PO19 8SQ, United Kingdom.
- Gabor, D. (1946), “Theory of communication”, *Proceedings of the IEEE 93(III)*, 429-457.
- Grossman, A. and Morlet, J. (1990), *Decompositions of functions into wavelets of constant shape and related transforms*, Mathematics and Physics – Lecture on Recent Results, World Scientific, Singapore, 135-65.
- Hahn, S.L. (1996), *Hilbert Transforms in Signal Processing*, Artech House (print-on-demand).
- Huang, N.E., Shen, Z., Long, S.R., Wu, M.C., Shih, H.H., Zheng, Q., Yen, N.C., Tung, C.C. and Liu, H.H. (1998), “The empirical mode decomposition and the Hilbert spectrum for nonlinear and non-stationary time series analysis”, *Philos. T. R. Soc. London A*, **454**, 903-995.
- Kareem, A. and Gurley, K. (1996), “Damping in structures: its evaluation and treatment of uncertainty”, *J. Wind Eng. Ind. Aerod.*, **59**(2-3), 131-157.
- Kawiecki, G. (2001), “Modal damping measurement for damage detection”, *Smart Mater. Struct.*, **10**(3), 466-471.
- Kijewski-Correa, T.L. (2003), *Full-scale measurements and system identification: a time-frequency perspective*, Ph.D. Dissertation, University of Notre Dame, Notre Dame, Indiana.
- Kijewski, T. and Kareem, A. (2003), “Wavelet transforms for system identification in civil engineering”, *Comput.-Aided Civil. Infrastruct. Eng.*, **18**(5), 339-355.
- Kullaa, J. (2003), “Damage detection of the z24 bridge using control charts”, *Mech. Syst. Signal. Pr.*, **17**(1), 163-170.
- Lardies, J. and Gouttebroze, S. (2002), “Identification of modal parameters using the Wavelet transform”, *Int. J. Mech. Sci.*, **44**(11), 2263-2283.
- Le, T.P. and Argoul, P. (2004), “Continuous Wavelet Transform for modal identification using free decay response”, *J. Sound Vib.*, **277**, 73-100.
- Le, T.P. and Paultre, P. (2012), “Modal identification based on continuous wavelet transform and ambient excitation tests”, *J. Sound Vib.*, **331**(9), 2023-2037.
- Lin, C.S. and Chiang, D.Y. (2012), “A modified random decrement technique for modal identification from nonstationary ambient response data only”, *J. Mech. Sci. Technol.*, **26**(6), 1687-1696.
- Loh, C.H., Mao C.H., Huang, J.R. and Pan, T.C. (2011), “System identification and damage evaluation of degrading hysteresis of reinforced concrete frames”, *Earthq. Eng. Struct. D.*, **40**(6), 623-640.
- McKenna, F., Fenves, G.L., Scott, M.H. and Jeremic, B. (2000), “Open system for earthquake engineering simulation – opensees”, <http://opensees.berkeley.edu>
- Michel, C. and Gueguen, P. (2010), “Time-frequency analysis of small frequency variations in civil engineering structures under weak and strong motions using a reassignment method”, *Struct. Health Monit.*, **9**(2), 159-171.
- Montejo, L.A. (2011), “Signal processing based damage detection in structures subjected to random excitations”, *Struct. Eng. Mech.*, **40**(6), 745-762.
- Montejo, L.A., Velazquez, L.R., Ramirez, R.I., Jiang, Z. and Christenson, R.E. (2012), “Frequency content effect on the efficiency of wavelet and hilbert-huang transforms for health monitoring”, *Proceedings of the 15th WCEE*, Lisbon, Portugal, September.
- Montejo, L.A. and Vidot, A.L. (2012), “Synchrosqueezed wavelet transform for frequency and damping identification from noisy signals”, *Smart Struct. Syst.*, **9**(5), 441-459.
- Park, Y. J. and Ang, A. H. S. (1985), “Mechanistic seismic damage model for reinforced concrete”, *J. Struct. Eng. - ASCE*, **111**(4), 722-739.

- Ramirez-Castro, R.I. and Montejo, L.A. (2011), "Hilbert Transform, empirical mode decomposition and its applications to free vibration analysis (in spanish)", *Revista Internacional de Desastres Naturales, Accidentes e Infraestructura Civil*, **11** (2), 123-134.
- Ruzzene, M., Fasana, A., Garibaldi, L. and Piombo, B. (1997), "Natural frequencies and dampings identification using Wavelet Transform: application to real data", *Mech. Syst. Signal. Pr.*, **11**(2), 207-218.
- Salawu, O.S. (1997), "Detection of structural damage through changes in frequency: a review", *Eng. Struct.*, **19**(9), 718-723.
- Schoettler, M.J., Restrepo, J.I., Guerrini, G., Duck, D.E. and Carrea, F. (2012), *A full-scale, single-column bridge bent tested by shake-table excitation*, Center for Civil Engineering Earthquake Research, Department of Civil Engineering, University of Nevada.
- Shi, W., Shan, J. and Lu, X. (2012), "Modal identification of Shanghai World Financial Center both from free and ambient vibration response", *Eng. Struct.*, **36**, 14-26.
- Staszewski, W.J. (1997), "Identification of damping in mdof systems using time-scale decomposition", *J. Sound Vib.*, **203**(2), 283-305.
- Todorovska, M.I. and Trifunac, M.D. (2007), "Earthquake damage detection in the imperial county services building I: the data and time frequency analysis", *Soil Dyn. Earthq. Eng.*, **27**(6), 564-576.
- Ülker-Kaustell, M. and Karoumi, R. (2011), "Application of the continuous wavelet transform on the free vibrations of a steel-concrete composite Railway Bridge", *Eng. Struct.*, **33**(3), 911-919.
- Ville, J. (1948), "Theorie et application de la notion de signal analytical (in French)", *Cables et Transmissions*, **2**(1), 61-74.
- Yan, B. and Miyamoto, A. (2006), "A comparative study of modal parameter identification based on Wavelet and Hilbert-Huang transforms", *Comput.-Aided Civil. Infrastruct. Eng.*, **21**(1), 9-23.
- Zembaty, Z., Kowalski, M. and Pospisil, S. (2006), "Dynamic identification of a reinforced concrete frame in progressive states of damage", *Eng. Struct.*, **28**(5), 668-681.